Proceedings of the ASME 2010 3rd Joint US-European Fluids Engineering Summer Meeting and 8th International Conference on Nanochannels, Microchannels, and Minichannels
FEDSM-ICNMM2010
August 1-5, 2010, Montreal, Canada

FEDSM-ICNMM2010-30718

A NOVEL MESHING APPROACH FOR LARGE EDDY SIMULATION

ZHANG Bin
Key Lab. for Power Machinery and Engineering,
Shanghai Jiao Tong University
Shanghai, China

WANG Tong
Key Lab. for Power Machinery and Engineering,
Shanghai Jiao Tong University
Shanghai, China

GU Chuan-gang
Key Lab. for Power Machinery and Engineering,
Shanghai Jiao Tong University
Shanghai, China

DAI Zheng-yuan
Trane's Asia-Pacific Research Center
Shanghai, China

ABSTRACT

In large eddy simulation (LES), the filtering grid scale (FGS) of LES equations is calculated generally by local mesh size. Therefore, proper LES Meshing is very decisive for better results and more economical cost. An effort was made to provide an available approach for LES meshing by turbulence theory and CFD methods. The expression for proper filtering grid scale (PFGS) was proposed on the basis of -5/3 law of inertial sub-range. A new parameter named grid ratio coefficient was put forward for the mesh adjustment. The proper mesh of LES could be built directly from the adjustment of RANS mesh. Two test cases both backward facing step flow and turbulent channel flow were provided to verify the approach. There were three kinds of mesh size, including coarse mesh for RANS (RCM), adjusted mesh for LES with the novel approach (NAM) and fine mesh for LES (LFM), employed here. The grid numbers of NAM were less than those of LFM evidently, and the results of NAM were in a good agreement with those of DNS and experiments. It was also revealed that results of NAM were very close to those of LFM. The conclusions provided positive evidences in the application of the approach.

1 INTRODUCTION

Under present computation performance, LES, as the transition between RANS and DNS, is a very promising and effective way to predict the turbulent flow relatively accurately [1]. The main thoughts of LES are to calculate large-scale fluctuations of the flow and model the effect of small-scale fluctuations [2]. These small-scale turbulent fluctuations and the influence between them could be obtained by sub-grid stress (SGS) models [3]. LES equations of the resolved turbulent scale are established by the low-pass spatial filtering of Navier-Stokes equations, so the filtering grid scale (FGS) of the spatial filter plays a decisive role for LES results [4]. The proper filtering grid scale (PFGS) should be within or close to the inertial sub-range of turbulence [4, 5]. However, FGS solutions of present SGS models were built up by the local computational mesh, such as Moeng C-H et al. [6], Metai O. et al. [7] and so on. It is probable for LES to make some great or unacceptable gaps between FGS of SGS models and PFGS because of improper mesh. It may lead to lose some useful small-scale fluctuations, fine description characteristics, economical cost advantage and the rationality of LES results. Therefore, the research on proper LES meshing was important and helpful for better turbulent data and more economical calculation.

Generally, most of prior suggestions [8] were adopted for LES meshing, such as following: the mesh near the wall should be refined; the mesh near the location of the great variable geometries should be refined; the mesh size should be located in the inertial sub-range, i.e. between the energy containing scale and the turbulent dissipation scale. However, they were some qualitative but not enough quantitative proposals, specially the central flow field outer boundary layer. Recently, the studies of LES meshing had been made the centre of discussion for more accurate LES data. Celik IB et al. [9],

Klein M [10] and Jordan SA [11] investigated the influence of LES mesh resolution and attempted to provide some sensitive ways to measure the quality of the LES predictions. The ways focused on that if the LES meshing was rational by analyzing the calculation results, but not the proper LES meshing before calculation. Gervasio Annes Degrazia et al. [12] offered the variable mesh spacing method for LES in the convective boundary layer, the method only provided the available meshing solution in the vertical direction yet. Yacine Addad et al. [13] mentioned a criterion for optimal unstructured meshing for LES based on Taylor micro-scales. It would help the further study on LES meshing obviously. Needed attentively, Taylor micro-scale was still located in the turbulent dissipation range [14], so the increased grid number of LES mesh might lose the original economic advantages. S. LEONARD et al. [15] addressed the problem of coupling an adaptive mesh refinement (AMR) method with LES. A multi-grid algorithm was used in order to refine the grid in zones detected by a specific sensor based on wavelet decomposition. Naudin A. et al. [16] also focused on AMR method with LES and proposed an available sensor defined by first calculated LES data of turbulent kinetic energy. However, AMR of LES was processed on the basis of the LES results of first mesh, but some criteria about the first mesh were not given quantitatively. It would not only increase the grid number of LES (Actually, there were twice LES calculation) but also lead to the irrational second AMR mesh because of the improper first mesh.

In this work, the efforts were made to provide an available approach or one more reference strategy for proper LES meshing and better LES data. Analyzed on the turbulent theory and CFD methods, a novel solution of PFGS was established. Then, a rational meshing approach for LES was proposed and the specific procedure was given here. The proper mesh of LES was generated by the adjustment of RANS mesh. Furthermore, two test cases both backward facing step flow (BFS) and turbulent channel flow (TCF) were applied for discussions and validations. The further researches were completed to offer creditable proofs in the application of the above approach.

The paper was organized as the following, Numerical methods including LES models and numerical details were described on Section 2; the detailed research on PFGS was carried out and an available LES meshing approach was attempted to put forward in Section 3; application of the approach to backward step facing flow was conducted and further discussions was given in Section 4; one more case for the application to turbulent channel flow and its validations was reported in Section 5; conclusions and acknowledgements were shown in Section 6 and Section 7, respectively.

2 NUMERICAL METHODS

2.1 LES Models

The solutions of LES are obtained on a relatively coarse grid (compared to DNS). To separate the large scales from the small scales, a filtering operation is conducted. The resolved part $\overline{\phi}(x_i)$ can be expressed:

$$\overline{\phi}(x_i) = \int \phi(\xi_i)\, \overline{H}(x_i - \xi_i, \Delta) d\xi_i \tag{1}$$

Where, ϕ is a generic variable, x_i and ξ_i are space vectors, $\overline{H}$ and Δ are the filtering function and filtering grid scale respectively. The filtering grid scale is a function of the grid resolution in present SGS models, and Δ is determined generally as following:

$$\Delta = \left(\Delta_x \Delta_y \Delta_z\right)^{1/3} \tag{2}$$

Where Δ_x, Δ_y and Δ_z is the grid widths in *x*, *y* and *z* respectively. The governing equations for LES are employed:

$$\left.\begin{aligned} &\frac{\partial \overline{u_i}}{\partial x_i} = 0 \\ &\frac{\partial \overline{u_i}}{\partial t} + \frac{\partial \overline{u_i}\,\overline{u_j}}{\partial x_j} = -\frac{1}{\rho}\frac{\partial \overline{p}}{\partial x_i} + \nu \frac{\partial^2 \overline{u_i}}{\partial x_j \partial x_j} - \frac{\partial \tau_{ij}}{\partial x_j} \\ &\tau_{ij} = \overline{u_i u_j} - \overline{u_i}\,\overline{u_j} \end{aligned}\right\} \tag{3}$$

Where, $\overline{u_i}$ is the filtered velocity field, x_j is the space vector, $\overline{p}$ is the pressure, ρ is the fluid density and ν is the kinematic viscosity of fluid. SGS stress τ_{ij} can describe the influence between small scales and large scales and is solved by SGS models. Most frequently-used SGS models are the models of eddy viscosity type.SGS stress τ_{ij} can be written as:

$$\tau_{ij} = \frac{1}{3}\tau_{kk}\delta_{ij} - 2\nu_t \overline{S}_{ij} \tag{4}$$

Where, the trace of SGS stress τ_{kk} is incorporated in the pressure resulting in a modified pressure term, ν_t is SGS kinematic viscosity, and δ_{ij} is the Kronecker delta function. $\overline{S}_{ij}$, the strain rate tensor for the large (resolved) scale, is defined as:

$$\overline{S}_{ij} = \frac{1}{2}\left(\frac{\partial \overline{u_i}}{\partial x_j} + \frac{\partial \overline{u_j}}{\partial x_i}\right) \tag{5}$$

Smagorinsky model (SM) [17, 18] is the most common SGS model in LES. In this model, sub-grid kinematic viscosity is modeled by:

$$\left.\begin{aligned} &\nu_t = \left(l_s\right)^2 \cdot \sqrt{2\overline{S}_{ij}\overline{S}_{ij}} \\ &l_s = \min\left(k_v y, C_s \Delta\right) \end{aligned}\right\} \tag{6}$$

Where, l_s is the mixing length for the SGS model, k_v is the von Karman constant (k_v=0.42), y is the distance to the nearest wall, Δ is the filtering grid scale, and C_s is Smagorinsky constant. In many studies of SM [19, 20], it is found that the Smagorinsky constant should be $C_s = 0.1 \sim 0.12$ for good results of a wide range of flows. In the present work of SM, C_s were selected as 0.1 for LES of turbulence.

2.2 Numerical Details

The code of RANS solver was based on a second order finite volume discretization, the SIMPLE pressure correction technique for enforcing the divergence-free condition of the velocity field. The time integration was three-level fully implicit. The eddy viscosity was obtained using the k-ε RNG model [21] with standard wall functions. The inlet velocity distribution was specified as that of a fully-developed turbulent flow at a same Re number. Structured grids were

used for the RANS simulations, and it was assured that *y* plus (<100) was proper for RANS simulation. The convergent results were got by the given residuals and the acceptable steady range of the monitory points.

The governing equations of LES were solved with a finite volume method using second-order central differences for diffusion terms and three-order QUICK differences for convective terms. Explicit second-order Runge-Kutta scheme was selected. Conservation of mass was achieved by the SIMPLE algorithm [22], with the Poisson equation solved by SIP procedure. SM SGS model was selected with the standard wall functions. The inlet velocity distribution was specified as that of a fully-developed turbulent flow at the same Reynolds number. The parallel solver was conducted on an Intel server which had 32GB RAM with two E5410 CPUs of 8 cores and the cost (time) for CFD simulation was shown in Tab.2.

3 THE NOVEL LES MESHING APPROACH

3.1 PFGS Solution

Based on the turbulence theory [14], there included energy containing range, inertial sub-range and dissipation range in the turbulent energy spectrum (shown in Fig.1). The famous kolmogorov –5/3 law could be given by:

$$E(k) = \alpha \cdot \varepsilon^{2/3} k^{-5/3} \tag{7}$$

Where, α, ε, k were kolmogorov constant (about 1.4), turbulent dissipation rate and wave-number respectively.

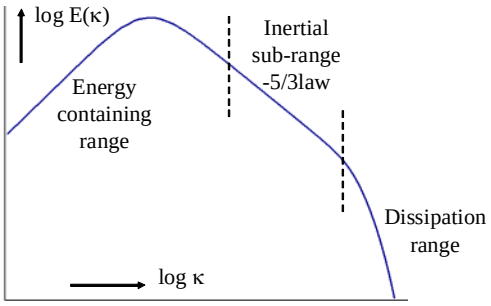

Fig.1 Turbulent energy spectrum

Assumed that the dissipation length-scale of fully developed turbulent flow was enough small, the wave-number range of inertial sub-range could be set: $[k_c, +\infty)$ .Eq. (7) was directly integrated:

$$\int_{k_c}^{+\infty} E(k)dk = 1.5 \cdot \alpha \cdot \varepsilon^{2/3} k_c^{-2/3} \tag{8}$$

It was noted that the left part of Eq. (8) was equal to sub-grid kinetic energy q_s in LES essentially, so we could get:

$$q_s = \int_{k_c}^{+\infty} E(k)dk \tag{9}$$

Eq. (8) and (9) led to:

$$k_c = (1.5\alpha)^{1.5} \cdot \varepsilon / q_s^{1.5} \tag{10}$$

The relations between wave-number k_c and space scale Δ_c in inertial sub-range (or local isotropy range) could be shown as:

$$k_c = \pi / \Delta_c \tag{11}$$

Eq. (10) and (11) led to:

$$\Delta_c = \left[\pi/(1.5\alpha)^{1.5}\right] \cdot q_s^{1.5} / \varepsilon \tag{12}$$

Eq. (12) could be rewritten as:

$$\Delta_c = \left[\pi/(1.5\alpha)^{1.5}\right] \cdot (q_s/K)^{1.5} \cdot K^{1.5} / \varepsilon \tag{13}$$

Where, K was the total turbulent kinetic energy, including energy containing range, inertial sub-range and dissipation range. Energy coefficient η_s , the ratio of sub-grid kinetic energy to total turbulent kinetic energy, was defined as:

$$\eta_s = q_s / K \tag{14}$$

According to LES theory [8], PFGS Δ was located in the local inertial sub-range. Therefore:

$$\Delta_c = \Delta = \left[\pi/(1.5\alpha)^{1.5}\right] \cdot \eta_s^{1.5} \cdot K^{1.5} / \varepsilon \tag{15}$$

It was shown that PFGS was related to energy ratio coefficient, total turbulent kinetic energy and turbulent dissipation rate. By using RANS model, K, ε could be calculated well. So that:

$$\Delta_c = \left[\pi/(1.5\alpha)^{1.5}\right] \cdot \eta_s^{1.5} \cdot K_{RN}^{1.5} / \varepsilon_{RN} \tag{16}$$

The "*RN*" subscript indicated that estimates of these quantities could be provided by RANS model.

3.2 Energy Ratio Coefficient Setting

By jointing LES principle with turbulence theory, the reasonable value or value range of η_s could be analyzed as follow:

Firstly, since the most turbulent kinetic energy was included in resolved scale of LES, the proper value should range from 0 to 0.5 firstly. The paper [3] concluded that LES should resolve at least 80% of the total turbulent kinetic energy.

Secondly, based on turbulence theory, the length-scale magnitude of energy containing range was higher than inertial sub-range. Energy containing length-scale could be expressed as:

$$l = C \cdot K^{1.5} / \varepsilon \tag{17}$$

Where, C was the constant taken close to the paper [23]. Eq. (15) and (17) led to:

$$\Delta_c / l = \pi \cdot \eta_s^{1.5} / \left[(1.5\alpha)^{1.5} \cdot C\right] \le 10^{-1} \tag{18}$$

The energy ratio should be:

$$\eta_s \le 0.196 \tag{19}$$

At last, the length-scale of inertial sub-range should be larger than Taylor dissipation micro-scale in turbulence. Taylor micro-scale could be written as:

$$\lambda = \sqrt{10K \cdot \upsilon / \varepsilon} \tag{20}$$

Where, υ was viscosity coefficient.

$$\Delta_c / \lambda \ge 1 \tag{21}$$

Eq. (15), (20) and (21) led to:

$$\eta_s \ge 1.96 / \left[C \cdot K^2 / (\varepsilon \cdot \upsilon)\right]^{1/3} \tag{22}$$

We define Reynolds number of energy containing range as:

$$\mathrm{Re}_l = \sqrt{K} \cdot l / \nu = C \cdot K^2 / (\varepsilon \cdot \upsilon) \tag{23}$$

Then,

$$1.96 / \mathrm{Re}_l^{1/3} \le \eta_s \le 0.196 \tag{24}$$

On the basis of the above discussion, for getting PFGS, a bound on energy ratio coefficient such as the following Eq. could be recommended:

$$\left.\begin{array}{ll} \eta_s = Mid\left[1.96/\mathrm{Re}_l^{1/3}, 0.196\right] & \mathrm{Re}_l > 10^3 \\ \eta_s = 0.196 & \mathrm{Re}_l \le 10^3 \end{array}\right\} \tag{25}$$

3.3 Meshing Procedure for LES

To match the computational mesh with PFGS in LES, an integrated LES meshing approach from RANS mesh adjustment was developed here. The procedure, as shown in Fig.2, could be described as following:

1) LES meshing problem should be established with the required detailed information such as computational fields, boundary conditions, etc.
2) RANS equations were solved by the specified turbulent model to get the needed turbulent flow information, including turbulent kinetic energy, dissipation rate and energy ratio coefficient.
3) PFGS Δ could be calculated by RANS results. Let's apply RANS mesh as the original LES mesh.
4) The filtering grid scale $\overline{\Delta}$ of SGS model was determined implicitly by local mesh size, as expressed as Eq. (2).
5) Grid ratio coefficient σ_Δ was defined as $\overline{\Delta}/\Delta_c$. The coefficient was selected as the mesh adjustor. Then, the σ_Δ distribution in the flow field could be got and the threshold value for mesh adjustment should be set.
6) This step was the convergence test 1: if the grid ratio coefficient of the total flow field was less than the threshold value (Selected as 1 in this work, sometime more according to the practical calculation demand).
7) If step 6) had not been true, the mesh of those non-satisfied fields should be refined by one-divided-into-two. The adjusted mesh would be the updated original LES mesh and a new process started form step 4). Otherwise, the process went into the next convergence test.
8) This step was the convergence test 2: if the relative difference of RANS results between the adjusted mesh and the original RANS mesh was less than the acceptable threshold value. (Selected as 5% in this work).
9) If step 8) had not been true, the adjusted mesh was set as the updated RANS mesh and a new process started form step 2). Otherwise, the process was over and the proper mesh for LES was obtained.

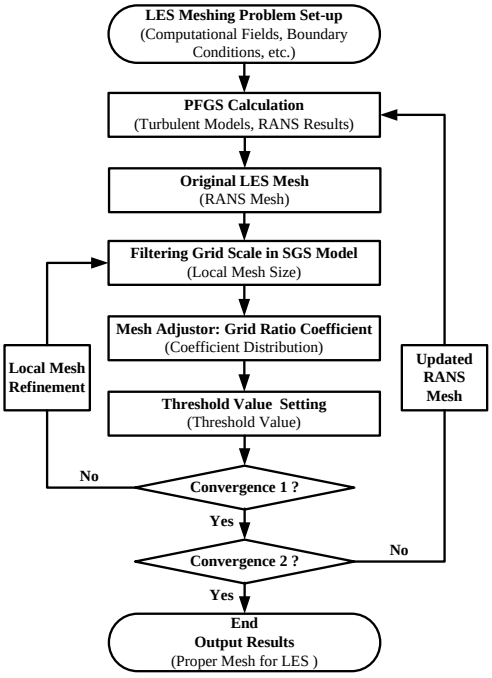

Fig.2 Meshing Procedure for LES

4 APPLICATION TO BACKWARD FACING STEP FLOW

To investigate the above mentioned approach, a benchmark case of the backward facing step flow (BFS) with SM were simulated at Re=5147. Many researchers [24-26] had conducted studies on this typical flow by using both experimental and numerical techniques. BFS included the separation of a turbulent boundary layer, reattachment of the boundary layer, recirculation, and the occurrence of secondary separation regions and so on. The schematic of BFS flow structure was shown in Fig.3, where the reattachment length, L, was related to Re and the expansion ratio H_2/H_1.

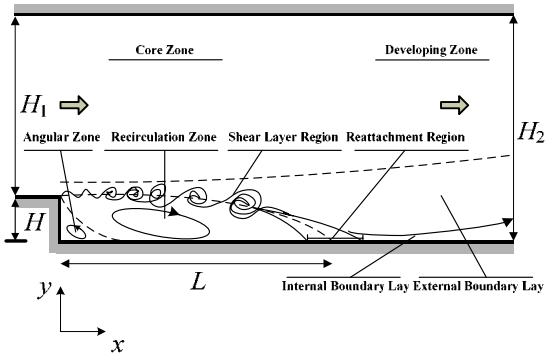

(a) Sketch of BFS Flow Structure

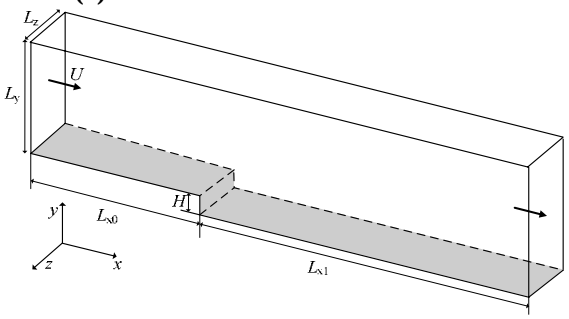

(b) Geometry of BFS

Fig.3 BSF Flow

Tab.1 BFS Flow Parameters

Properties	Symbol	Re=5147, H_2/H_1=1.2
Inlet Velocity	U	$7.72m/s$
Step Height	H	$0.0098m$
Reattachment Length	L	$5.3H(RCM)$ $6.7H(NAM)$ $6.9H(LFM)$
x Length	L_{x0} L_{x1}	$0.0980m$ $0.1960m$
y Length	L_y	$0.0588m$
z Length	L_z	$0.0392m$
Kinetic Viscosity	ν	$1.47\times10^{-5}m^2/s$

The computational domain of BFSF was represented in Fig.3. The main parameters of the test case were described in Tab.1. Where, structured grids were used for the RANS simulations presented. Non-uniform grid cells were adopted in x and y directions while uniform grid cells were used in z direction.

The grid near wall was refined. To offer the valid data for LES meshing, RANS mesh was obtained by the grid independence with the separation point location as the test quantity. The boundary conditions of BFS were expressed: inlet boundary: velocity inflow; outlet boundary: sommerfeld radiation condition; upper boundary: symmetrical boundary condition; inner and outer boundary in *z*-direction: periodic boundary condition; the other boundaries: no slip boundary condition.

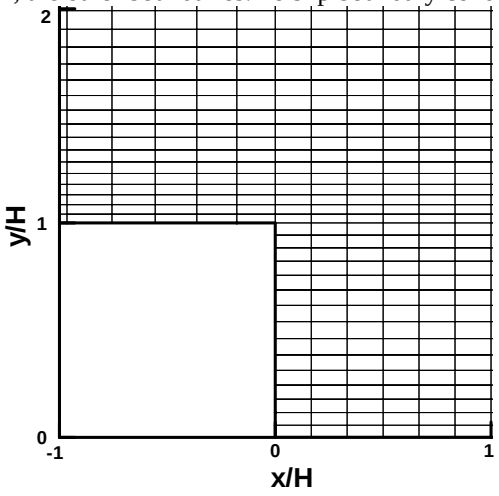

(a) RANS Mesh near the Step

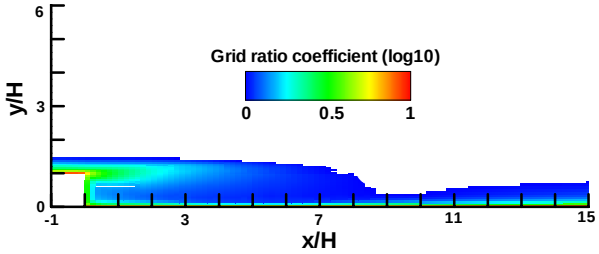

(b) RANS: Grid Ratio Coefficient

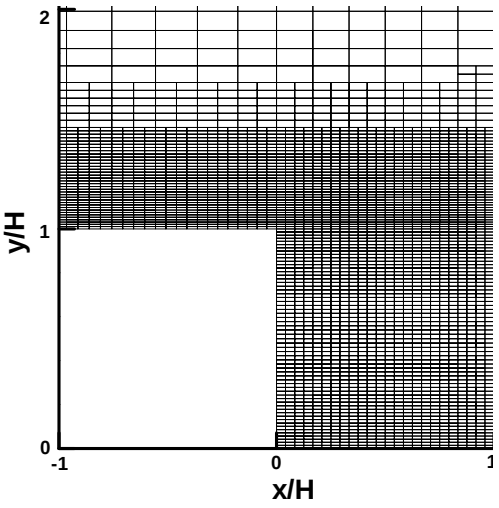

(c) Adjusted Mesh for LES near the Step

Fig.4 LES Meshing of BFS

For the convenient study, the flow of mid section in *z* direction was selected for description. RANS mesh near the step, RANS-based results: the grid ratio coefficient and the adjusted mesh for LES were illustrated in Fig.4. The results shown that the local mesh needed to be adjusted in angular zone, recirculation zone, partial shear layer region, reattachment region and internal boundary lay. The grid numbers of the final LES mesh were about 0.42 million. Three kinds of mesh size (Tab.2), including RCM, NAM and LFM, were employed for comparison and validation. It was shown that the numbers of NAM was less than those of LFM and DNS evidently. In LES, the time step was 0.05 non-dimensional times. Time averaging was obtained for 500 non-dimensional times and spatial averaging was accomplished at the last time step.

LES simulations of BFS were carried out for NAM and LFM. Different flow parameters, reattachment length, mean velocity profiles, turbulent intensity and Reynolds shear stress were computed and compared with DNS data of Le et al. [25] and experimental data of Jovic et al. [26], as illustrated in Tab.1 and Fig.5-Fig.8. These parameters were averaged in time and along the spanwise direction. Mean velocity profiles, turbulent intensity and Reynolds shear stress were nondimensionalize with inflow free stream velocity. Fine, but not same accordance could be seen between the experimental and DNS data. However, DNS and experimental data could be combined to verify LES data better.

Tab.2 Different Considered Meshes

Mesh	Details Parameters	BFS	TCF
RCM	Grid Number	0.05million	0.03million
	Model	k-ε RNG	k-ε RNG
	Cost-Time	≈ 3 hours	≈ 1 hour
NAM	Grid Number	0.42million	0.19million
	Model	SM	SM
	Cost-Time	≈ 8 days	≈ 3 days
LFM	Grid Number	1.18million	0.53million
	Model	SM	SM
	Cost-Time	≈ 23 days	≈ 8 days
DNS	Grid Number	9.44million	3.93million
	Model	-	-

Based on LES results, DNS and experimental data, the detailed conclusions were expressed as following:

1) Reattachment Length

The mean reattachment length L was obtained by the method (Longitudinal distance where mean longitudinal velocity u=0 at the first grid point normal to the wall) as proposed by Le et al. [25]. The reattachment lengths of RCM, NAM and LFM were 5.3H, 6.9H and 6.7H respectively. LES results, better than RANS data, was relatively close to the DNS value (6.28H) and the experimental value (6H). However, Increase of LES reattachment length might be caused due to the absence of the turbulent longitudinal vortices' associated with the inflow boundary layer [27]. LES data of Dubief and Delcayre [28] showed a recirculation length of 7.2H at the same Re of 5100, and the inflow boundary condition was mean velocity profile perturbed with white noise. Simons et al. [24] also carried out LES over BFS and they observed the recirculation length of 6.6H with SM. It was supported that LES results for the reattachment length was usually longer.

2) Mean Velocity Profiles

Fig.5 showed the comparison among the computed LES data (NAM and LFM), DNS and experimental data for the non-dimensional mean stream velocity profiles. The comparison was made at four locations in the recirculation zone (x/H=4), reattachment region (x/H=6) and recovery

regions (x/H=10 and x/H=19), where DNS and experimental data were available.

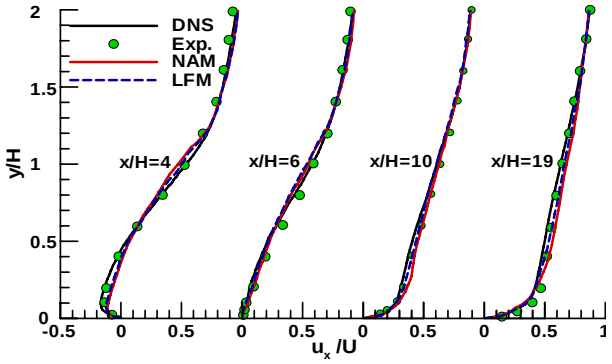

Fig.5 Mean streamwise velocity

Discrepancy between the mean velocity profiles of the DNS by Le et al and the experiments of Jovic and Driver was observed, especially for the region y/H<1. But, the difference between them didn't affect the following validation. At x/H=4, the results of LES were over-predicted in the region y/H<0.5 and under-predicted in the region 0.5<y/H<1 relatively. The computed LES results of NAM and LFM compared well with the DNS results at x/H=6. The stream velocity of LES data was over-predicated slightly at x/H=10, especially y/H<0.5. It was observed that the stream velocity of LES data was over-predicated at x/H=19, y/H<1.5. On the whole, the results of NAM were in a relatively good agreement with those of DNS and experiments. It was also found that the results of NAM with relatively less cells were nearly consistent to those of LFM.

3) Turbulent Intensity and Reynolds Shear Stress

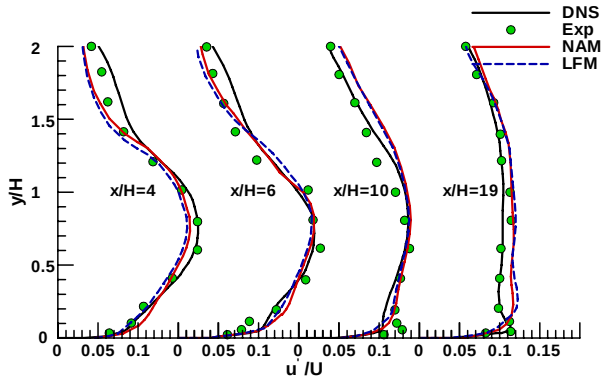

Fig.6 Streamwise Turbulent Intensity

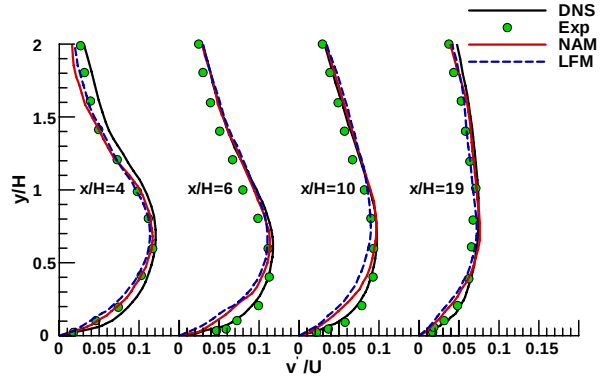

Fig.7 Normal Turbulent Intensity

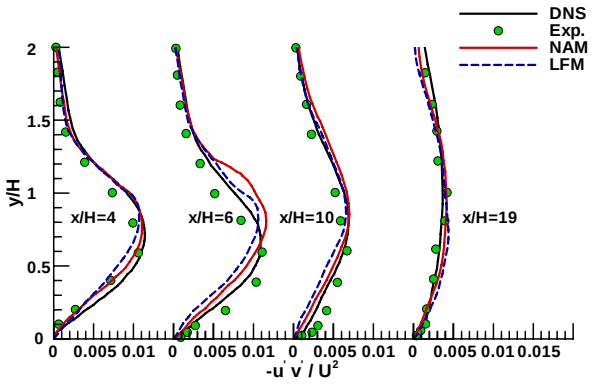

Fig.8 Reynolds Shear Stress

Fig.6-Fig.8 expressed streamwise turbulent intensity, normal turbulent intensity and Reynolds shear stress, as compared to DNS and experimental data, where u' and v' were the velocity fluctuation in streamwise and normal direction respectively. The comparison was made at the same four locations. When x/H=4 and 6, the streamwise turbulent intensity of LES data (NAM and LFM) predicted well with DNS especially for the region y/H<1.25 and was under-predicted for the other region. At recovery region (x/H=10 and 19), It was well close at y/H<1was and slightly over-predicted at y/H>1. When x/H=4, the normal turbulent intensity of LES was under-predicted but relatively close to those of experiments. When x/H=6, 10 and 19, the results of LES compared well with those of DNS at y/H>1 and under-predicted at the other region. As for Reynolds shear stress, the data of LES was only under-predicted for the region y/H<1 at x/H=4. The results of LES was under-predicted for the region y/H<0.75 and over-predicted for the region 0.75<y/H<1.5 at x/H=6. And the good agreements were shown at x/H=10 and 19. Actually, those of NAM were a little superior to the results of LFM. When the grid numbers of NAM were less than those of LFM evidently, the results of NAM were very close to those of LFM and in a good agreement with those of DNS and experiments. The above conclusion proved the rationality and validity of the novel LES meshing approach.

5 APPLICATION TO TURBULENT CHANNEL FLOW

In this section, the above approach was applied to LES of a turbulent channel flow (TCF) for further research, where SM SGS model had been used. TCF, as shown in Fig.9, was also a standard test case with available DNS data [29] and experimental data [30]. The channel was bounded only in the normal (y) direction and extended to infinity in streamwise (x) and spanwise (z) directions. The model was built for a channel of $(4\pi H \times 2H \times 2\pi H)$ at $\mathrm{Re}_\tau = 180$ (based on the friction velocity u_τ and the half channel width H). The half channel width was H=1 here.

The structured grids were plotted for the RANS simulations. Uniform grid cells were used in x and z directions, while stretched grid cells in y direction [31]. RANS mesh was obtained by coarsening DNS mesh by a factor of 6 in each direction. The domain was divided into (32×22×28) cells in x, y and z directions respectively. Periodic boundary conditions were set in x and z directions, no slip boundary conditions were used in y-direction.

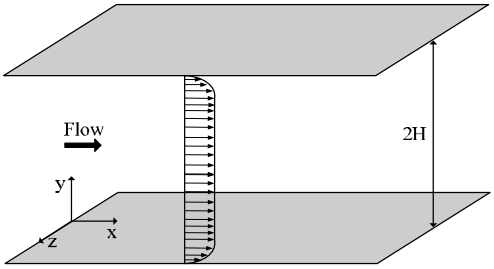

Fig.9 Geometry of TCF

The calculated LES results were illustrated in Fig.10-Fig.14 respectively, as compared with the DNS results of Kim et al. [29] and the experimental results of Niederschulte et al. [30]. The DNS study employed about 4 million grid numbers ((192 ×129×160) cells in *x*, *y* and *z* directions respectively). The experimental results were performed specifically to examine the accuracy of DNS results. The experimental results are close to those of DNS, but not exactly same.

Based on the above meshing procedure, LES mesh was obtained by adjusting RANS mesh. The final grid numbers were about 0.19 million. Three kinds of mesh size (Tab.2) including relatively coarse mesh for RANS (RCM), adjusted mesh for LES with the novel approach (NAM) and fine mesh (coarsening DNS mesh by a factor of 2 in each direction) for LES (LFM) were employed for evaluation and validation. It was found that the numbers of NAM was less than those of LFM and DNS evidently. Furthermore, the time step was 0.009 non-dimensional times. Time averaging was carried out for 50 non-dimensional times and spatial averaging was conducted at the last time step.

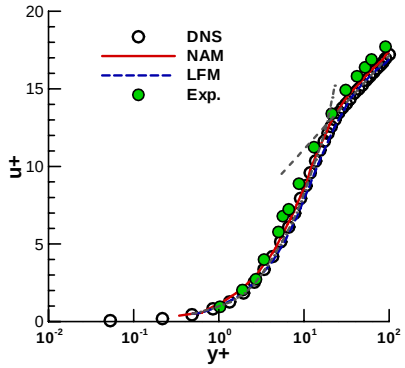

Fig.10 Mean streamwise velocity

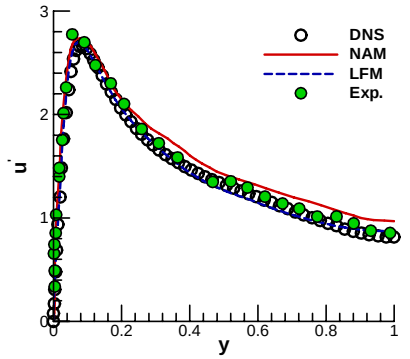

Fig.11 RMS of Streamwise Velocity Fluctuations

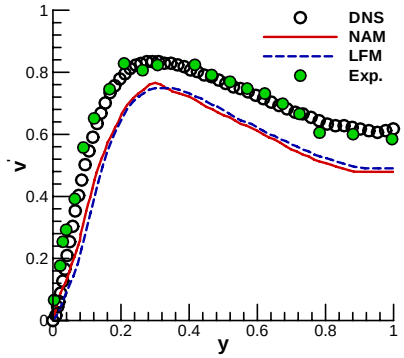

Fig.12 RMS of Normal Velocity Fluctuations

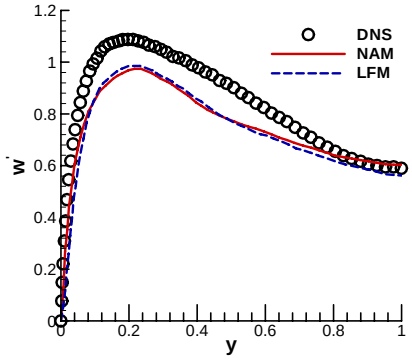

Fig.13 RMS of Spanwise Velocity Fluctuations

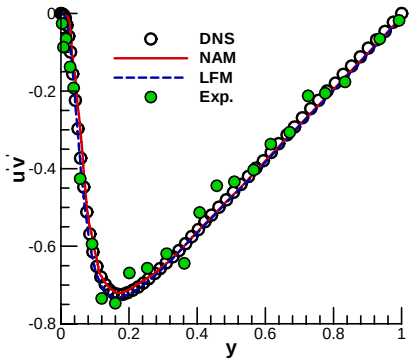

Fig.14 Reynolds Shear Stress

By averaging in the homogeneous directions (*x* and *z*) and time (*t*), the mean streamwise velocity profile near wall coordinates was shown in Fig.10. The mean velocity was normalized by the friction velocity as $u^+ = u/u_\tau$. The dashed gray-line and the dash-dotted gray-line represented the law of the wall and the logarithm law, respectively. It could be found that LES results of NAM and LFM agreed well with the DNS and experimental data in the mean streamwise velocity. The normalized RMS velocity fluctuations were shown in Fig.11-Fig.13. The results revealed that the results of NAM were very close to those of LFM. The results of LES (NAM and LFM) were in relatively good agreement with those of DNS and experiments. However, there still existed some gaps between them, since LES data represented the resolved scale intensities and didn't include the small-scale contribution.

The normalized Reynolds shear stress was shown in Fig.14. It was also expressed that LES results of NAM matched well with DNS data and a little superior to those of LFM.

Therefore, it was obtained that the results of NAM with relatively less cells were nearly same with those of LFM and were a good consistent to those of DNS and experiments. Therefore, the research conclusions of BFS and TCF provided the confidence in the application of the novel approach.

6 CONCLUSIONS

In this paper, an available LES meshing approach was developed. Both turbulence theory and CFD methods were employed in this approach. Through the above analysis, the following remarks could be obtained.

1) Based on turbulence theory, a novel expression for proper filtering grid scale (PFGS) was put forward on the basis of -5/3 law of inertial sub-range. It was found that PFGS was related to turbulent kinetic energy (k), turbulent dissipation rate (ε) and energy ratio coefficient (η_s). k and ε could be obtained from RANS data. A bound for η_s was established by the analysis on different turbulent scales.
2) To match LES computational mesh with PFGS for more accurate results, an integrated LES meshing approach was proposed and the detailed procedure was given here. The grid ratio coefficient was selected as the parameter for the mesh adjustment. The proper mesh of LES could be generated from the adjustment of RANS mesh.
3) Two benchmark cases both backward facing step flow (BFS) and turbulent channel flow (TCF) were tested to discuss and verify the above approach. Three kinds of mesh size, including RCM, NAM and LFM, were employed for the comparison and analysis of mean velocity, turbulent intensities and Reynolds shear stress here. It was shown that the grid numbers of NAM were less than those of LFM obviously and the results of NAM were very close to those of LFM. The results were in a good agreement with those of DNS and experiments.

NOMENCLATURE

BFS	Backward facing step flow
DNS	Direct numerical simulation
FGS	Filtering grid scale
LES	Large eddy simulation
LFM	Fine mesh for LES
NAM	Adjusted mesh for LES with the novel approach
PFGS	Proper filtering grid scale
RANS	Reynolds-average Navier-Stokes equations
RCM	Coarse mesh for RANS
SGS	Sub grid stress
SM	Smagorinsky model
TCF	Turbulent channel flow
C	Constant
C_s	Smagorinsky constant
E	Turbulent energy spectrum
$\bar{H}$	Filtering function
H	Step Height of BFS ; half channel width of TCF
H_2/H_1	Expansion ratio of BFS
K	Total turbulent kinetic energy
K_{RN}	Turbulent kinetic energy of RANS
l	Energy containing length scale
l_s	Mixing length
L	Reattachment length of BFS
L_{x0} L_{x1}	x Length of BFS
L_y	y Length of BFS
L_z	z Length of BFS
$\overline{p}$	Pressure
q_s	Sub-grid kinetic energy
Re_l	Reynolds number
Re_τ	Reynolds number of TCF
$\overline{S}_{ij}$	Strain rate tensor
u_τ	Friction velocity of TCF
u	Mean velocity of TCF
u^+	Normalized mean velocity of TCF
U	Inlet Velocity of BFS
u_x	Mean streamwise velocity of BFS
u'	Velocity fluctuation in streamwise
$-\overline{u'v'}$	Reynolds shear stress
$\overline{u}_i$	Filtered velocity field
v'	Velocity fluctuation in normal direction
x, y, z	Direction
x_i , x_j	Space vectors
y	The distance to the nearest wall
α	Kolmogorov constant
δ_{ij}	Kronecker delta function
$\overline{\Delta}$	Present filtering grid scale of SGS model
Δ	Filtering grid scale of LES
Δ_x , Δ_y , Δ_z	Grid widths in x, y and z respectively
Δ_c	Space scale in inertial sub-range
ε	Turbulent dissipation rate
ε_{RN}	Turbulent dissipation rate of RANS
η_s	Energy coefficient
k_v	Von Karman constant
k_c	Wave-number in inertial sub-range
k	Wave-number
ν	Kinematic viscosity
ν_t	SGS kinematic viscosity
ξ_i	Space vectors
ρ	Fluid density
σ_Δ	Grid ratio coefficient
τ_{ij}	SGS stress
ϕ	A generic variable

ACKNOWLEDGE

This research was supported by National Science Foundation under grant No. 50776056.

REFERENCE

[1]. Marcel Lesieur, 2008. Turbulence in fluids [M]. Springer Press (Netherland).
[2]. Muschinski A, 1996. A similarity theory of locally homogeneous and isotropic turbulence generated by Smagorinsky-type LES. J Fluid Mech, 325, pp.239-260.
[3]. Pope SB, 2004. Ten questions concerning the large-eddy simulation of turbulent flows. New J Phys, 6, pp.1-24
[4]. L. C. Berselli et.al, 2009. Mathematics of Large Eddy Simulation of Turbulent Flows [M], Springer press.
[5]. Mason PJ, 1994. Large-eddy simulation: a critical review of technique. Q J Roy Meteorol Soc, 120, pp.120:1-26.
[6]. Moeng C-H, Wyngaard JC, 1988. Spectral analysis of large-eddy simulations of the convective boundary layer. J Atmos Sci, 45, pp.3575-3587.
[7]. Metai O. Ferziger J H., 1997. New tools in turbulence modeling [M].Springer.
[8]. P. SAGAUT, 2002. Large eddy simulation for incompressible flows [M], Springer press.
[9]. Celik IB, Cehreli ZN, Yavuz I, 2005. Index of resolution quality for large eddy simulations. Journal of Fluids Engineering, 127, pp.949-958.
[10]. Klein M, 2005. An attempt to assess the quality of large eddy simulations in the context of implicit filtering. Flow, Turbulence and Combustion, 75, pp.131-147.
[11]. Jordan SA, 2005. A priori assessments of numerical uncertainty in large-eddy simulations. Journal of Fluids Engineering, 127 (6), pp.1171-1182.
[12]. Gervasio Annes Degrazia et al., 2009. A Variable Mesh Spacing for Large-Eddy Simulation Models in the Convective Boundary Layer. Boundary-Layer Meteorol, 131, pp.277-292.
[13]. Yacine Addad, Ulka Gaitonde, Dominique Laurenc, 2008. Optimal Unstructured Meshing for Large Eddy Simulations, Quality and Reliability of LES, 12, pp.93-103.
[14]. Frisch U, 1995. Turbulence: The Legacy of A.N. Kolmogorov [M]. Cambridge University Press.
[15]. S. Lonard, M. Terracol, P. Sagaut, 2006. A wavelet-based adaptive mesh refinement criterion for large-eddy simulation, Journal of Turbulence, 64 (7), pp.1–25.
[16]. Naudin, A., Vervisch, L., Domingo, P.A, 2007. Turbulent-Energy Based Mesh Refinement Procedure for Large Eddy Simulation. Advances in Turbulence XI: Proceedings of the 11th EUROMECH European Turbulence Conference, pp.413-415.
[17]. Smagorinsky, J, 1963. General circulation experiments with the primitive equations, I. the basic experiment. Monthly Weather Review, 91, pp. 99-164.
[18]. LILLY D. K., 1992. A proposed modification of the Germano sub-grid scale closure method. Physics of Fluids, 4(3), pp.633-635.
[19]. ZHAO Wei, Huhe Aode, 2006. Large-eddy simulation of three-dimensional turbulent flow around a circular pier. Journal of Hydrodynamics, Ser. B, 18(6), pp.765- 772.
[20]. XU Chang-yue, CHEN Li-wei, LU Xi-yun, 2007. Large-eddy and detached-eddy simulations of the separated flow around a circular cylinder Journal of Hydrodynamics, Ser. B, 19(5), pp. 559-563.
[21]. F.S Lien and M.A. Leschziner, 1994. Assessment of turbulence-transport models including non-linear RNG eddy viscosity formulation and second moment closure for flow over a backward-facing step. Computers and Fluids, 23, pp. 983-1004.
[22]. SUKSANGPANOMRUNG, 1999. A. Investigation of unsteady separated flow and heat transfer using direct and large-eddy simulations [D]. Ph. D. Thesis, Victoria, Australia: University of Victoria.
[23]. Kang HS, Chester S, Meneveau C, 2003. Decaying turbulence in an active-gridgenerated flow and comparisons with large-eddy simulation. Journal of Fluid Mechanics, 480, pp.129-160.
[24]. E.Simons, M.Manna, C.Benocci, 2002. Parallel multidomain large-eddy simulation of the flow over a backward facing step at Re=5100. Advances in LES of Complex F1ows, Springer, pp. 115-130.
[25]. Hung Le, Parviz Moin, 1997. Direct numerical simulation of turbulent flow over a backward-facing step. Journal of Fluid Mechanics, 330, pp. 349-374.
[26]. Jovic S., Driver D M, 1994. Backward-facing step measurement at low Reynolds number. NASA Tech. Mem. 108807.
[27]. M.Lesieur, O.Metais, P.Comte, 2005. Large-Eddy Simulations of Turbulence [M]. Cambridge University Press.
[28]. Y.Dubief, F.Delcayre, 2000. On coherent-vortex identification in turbulence. Journal of Turbulence, l, pp. 1-22.
[29]. Kim J, Moin P, Moser R, 1987. Turbulence statistics in fully developed channel flow at low Reynolds number, Journal of Fluid Mechanics, 177, pp.133-166.
[30]. Niederschulte MA, Adrian RJ, Hanratty TJ, 1990. Measurements of turbulent flow in a channel at low Reynolds numbers, Experiments in Fluids, 9, pp.222-230.
[31]. Moin P, Kim J, 1982. Numerical investigation of turbulent channel flow, Journal of Fluid Mechanics, 118, pp.341-377.